Chemistry–A European Journal
Research Article
doi.org/10.1002/chem.202400048
Chemistry Europe
European Chemical Societies Publishing
www.chemeurj.org

Morphological Transformations of SARS-CoV-2 Nucleocapsid Protein Biocondensates Mediated by Antimicrobial Peptides

Marco Campanile,[a] Emine Dila Kurtul,[b] Robert Dec,[c] Simone Möbitz,[c] Pompea Del Vecchio,[a] Luigi Petraccone,[a] Jörg Tatzelt,[b] Rosario Oliva,*[a] and Roland Winter*[c]

Recently, the discovery of antimicrobial peptides (AMPs) as excellent candidates for overcoming antibiotic resistance has attracted significant attention. AMPs are short peptides active against bacteria, cancer cells, and viruses. It has been shown that the SARS-CoV-2 nucleocapsid protein (N–P) undergoes liquid-liquid phase separation in the presence of RNA, resulting in biocondensate formation. These biocondensates are crucial for viral replication as they concentrate the viral RNA with the host cell's protein machinery required for viral protein expression. Thus, N–P biocondensates are promising targets to block or slow down viral RNA transcription and consequently virion assembly. We investigated the ability of three AMPs to interfere with N–P/RNA condensates. Using microscopy techniques, supported by biophysical characterization, we found that the AMP LL–III partitions into the condensate, leading to clustering. Instead, the AMP *Cr*ACP1 partitions into the droplets without affecting their morphology but reducing their dynamics. Conversely, GKY20 leads to the formation of fibrillar structures after partitioning. It can be expected that such morphological transformation severely impairs the normal functionality of the N–P droplets and thus virion assembly. These results could pave the way for the development of a new class of AMP-based antiviral agents targeting biocondensates.

In late 2019, the SARS-CoV-2 pandemic started, causing millions of deaths worldwide.[1] The SARS-CoV-2 is a single-stranded RNA virus whose genetic material is protected by the nucleocapsid protein (N–P, Figure 1A).[2] The N–P is overexpressed in infected cells and plays a key role in virion assembly.[3,4] N–P has been shown to undergo liquid-liquid phase separation (LLPS),[4,5] forming biocondensates in which the viral RNA and host cell protein machinery necessary for its transcription are concentrated, promoting the formation of new viruses.[6] Therefore, targeting N–P/RNA biocondensates is a promising strategy to slow down or block viral replication.

[a] *M. Campanile, Prof. Dr. P. Del Vecchio, Prof. Dr. L. Petraccone, Dr. R. Oliva*
Department of Chemical Sciences,
University of Naples Federico II,
Via Cintia, 26, 80126, Naples (Italy)
E-mail: rosario.oliva2@unina.it

[b] *E. D. Kurtul, Prof. Dr. J. Tatzelt*
Department Biochemistry of Neurodegenerative Diseases,
Institute of Biochemistry and Pathobiochemistry,
Ruhr University Bochum, 44801, Bochum (Germany)

[c] *Dr. R. Dec, S. Möbitz, Prof. Dr. R. Winter*
Physical Chemistry I – Biophysical Chemistry,
Department of Chemistry and Chemical Biology,
TU Dortmund University, Otto-Hahn-Strasse 4a,
44227, Dortmund (Germany)
E-mail: roland.winter@tu-dortmund.de

Supporting information for this article is available on the WWW under https://doi.org/10.1002/chem.202400048

Antimicrobial peptides (AMPs) are short peptides that act against pathogens including bacteria, cancer cells, and viruses.[7,8] Effective AMPs are characterized by a broad spectrum of antimicrobial activities, high pathogen specificity, and low toxicity. In addition, AMPs have been found to be involved in a variety of biological functions, including immune regulation, angiogenesis, wound healing, and antitumor activity.[8–10] Many AMPs act by perturbing the membrane lipid matrix, but some of them can translocate into the cytoplasm, targeting intracellular components such as proteins, nucleic acids, and organelles.[8,9] AMPs with antiviral activity are mostly associated with viral assembly, adsorption, and entry processes, in addition to their ability to target the nucleic acids of viruses.[10] Some designed synthetic peptides have been reported to inhibit SARS-CoV-2 infection by targeting certain viral proteins and, thus, blocking virus entry into the host cell,[11] as exemplified by the binding of *in silico*-designed ΔABP–D25Y to the S-protein.[12] Given the high mutation rate of the viral genome, peptide resistance can easily develop.[13] Therefore, complementary approaches are needed. One alternative is to use AMPs to target biocondensates of viral proteins and RNAs, whose partitioning is controlled by the physicochemical properties of the peptides rather than by specific binding to viral proteins.

Here we investigated the ability of three AMPs, LL–III, GKY20, and *Cr*ACP1 (Figure 1B), to interfere with the condensates formed by the N–P and polyU (800 kDa), the latter serving as a model for the viral RNA. These peptides exert their function through different action mechanisms. LL–III is extracted from the venom of the bee *Lasioglossum laticeps* and is active against bacteria and cancer cells.[16,17] LL–III translocates across the

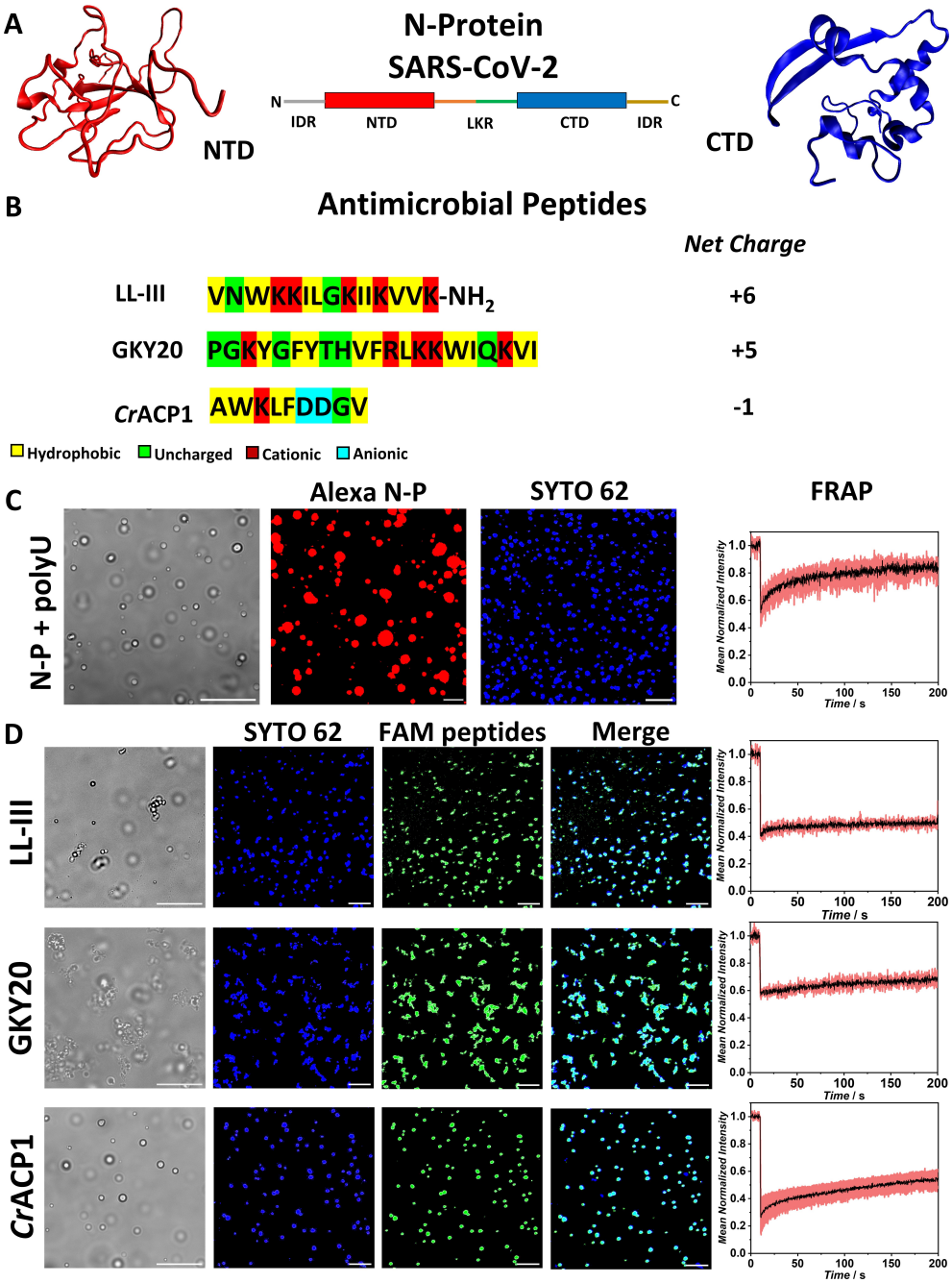

Figure 1. (A) Schematic representation of the N–P from SARS-CoV-2. The sequence is composed of intrinsically disordered regions (IDR) located at the N-, C-terminus and in the middle (LKR). The orange region of LKR is enriched in S and R residues. The N–P has two folded regions, NTD (pdb: 6YI3)[14] and CTD (pdb: 7CE0),[15] whose structures are shown. (B) Sequences of the antimicrobial peptides used in this study. Light and fluorescence microscopy snapshots and FRAP recovery plots of Alexa647-labelled N–P of (C) N–P/polyU pure droplets (10 μM/50 nM) and (D) N–P/polyU droplets upon addition of the peptides (100 μM). The polyU was stained with SYTO62 (in blue), the peptides labelled with FAM (in green) and the N–P with Alexa647 (in red). The merged pictures are the superimposition of the fluorescence of SYTO62 and FAM. Additional microscopy images are shown in Figs. S1-4. The red shadows in the FRAP plots are the standard deviations on the recorded intensities. All the experiments were performed at room temperature (25 °C) in 20 mM HEPES buffer, pH 7.4. Scale bars: 20 μm.

membrane of cancer cells, localizing in the nucleoli biocondensate.[17] LL–III has also been reported to perturb droplets of LAF-1 as well as the droplet-to-fibril transition of α-synuclein.[18,19] *Cr*ACP1 is a plant-derived peptide capable of killing cancer cells by disrupting their nucleosome,[20] a fluid-like structure involved in the regulation of chromatin phase separation.[21] Finally, GKY20 is a human thrombin-derived peptide[22] which acts against bacteria, destroying the lipid matrix of their membrane.[23] The aim of this study was to test the effect of these different AMPs on the stability and morphology of N–P/polyU condensates.

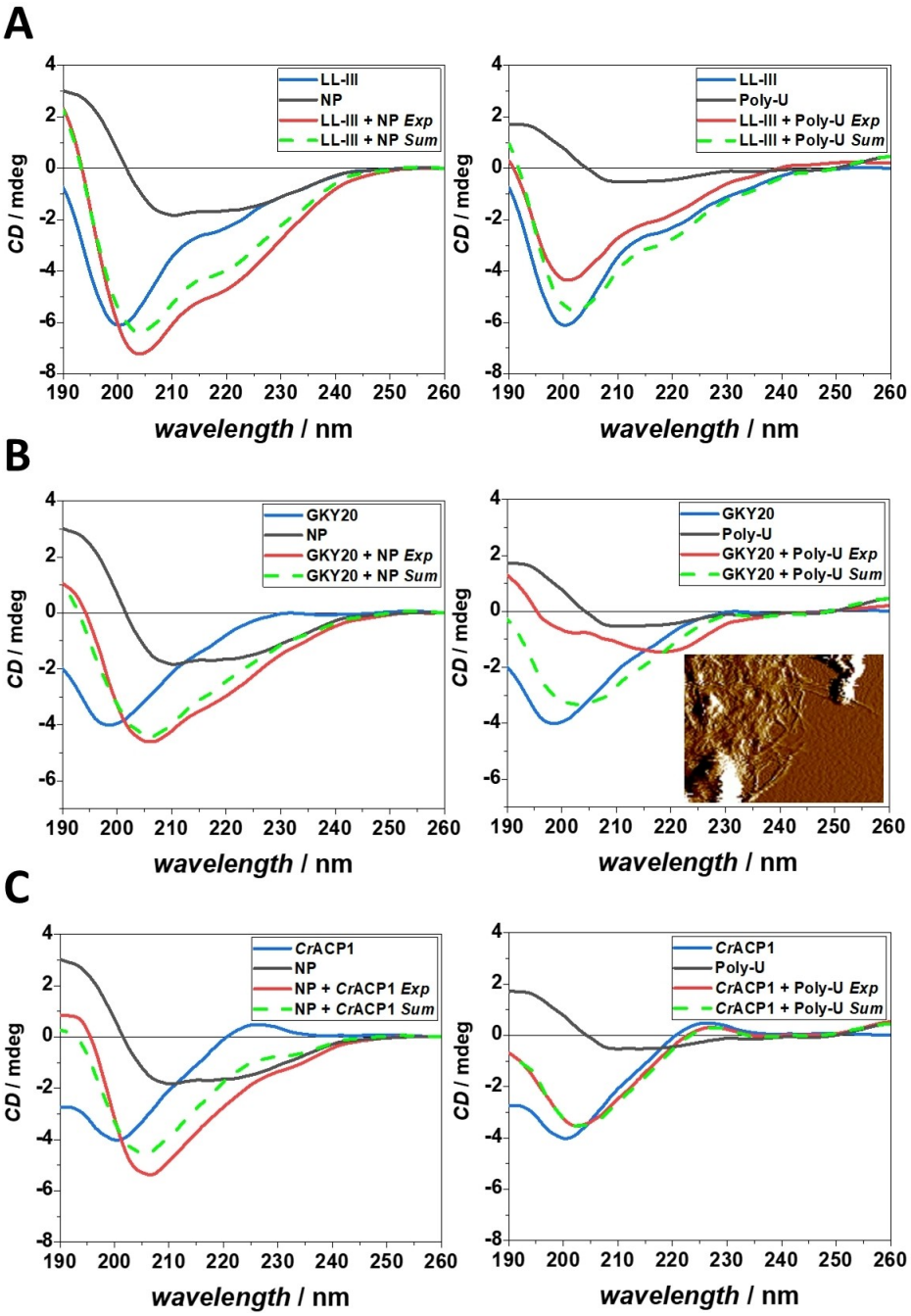

Figure 2. Circular dichroism (CD) spectra of (A) LL–III, (B) GKY20, and (C) CrACP1 mixed with N–P (left panel, red lines) and mixed with polyU (right panel, red line). For comparison, the spectra of N–P, polyU, and the peptides are also shown. The dashed green lines are the spectra obtained from the sum of the spectra of peptides and N–P (or polyU) recorded separately. All the peptides adopt a random coil conformation, as evidenced by the minimum around 200 nm The spectrum of N–P shows two minima (around 222 nm and 208 nm) and a maximum around 195 nm, suggesting the presence of a helical structure with contributions from β-sheets and unordered regions. The experiments were performed at 25 °C in 20 mM Hepes buffer, pH 7.4.

Figure 1C shows a light microscopy snapshot of N–P mixed with polyU, showing μm-sized droplets, as previously reported.[4] RNA co-localization within the droplets was confirmed by confocal fluorescence microscopy (Figure 1C), using the dye SYTO62 which selectively stains the polyU.[24] We then evaluated the impact of the three AMPs on the morphology of N–P/polyU condensates at increasing peptide concentrations (from 10 μM to 100 μM) using different microscopy techniques (Figs. 1D and S1, S2 and S3). Both LL–III and GKY20 induced the formation of irregular structures, including droplet association, with GKY20 showing a more pronounced effect at the lowest concentration used (Figs. S1 and S2). Conversely, *Cr*ACP1 had no effect on the morphology of the N–P/polyU condensates, even at 100 μM (Figs. 1D and S3). However, the fluorescence microscopy experiments performed with SYTO62 and FAM-labelled peptides showed co-localization also of this peptide

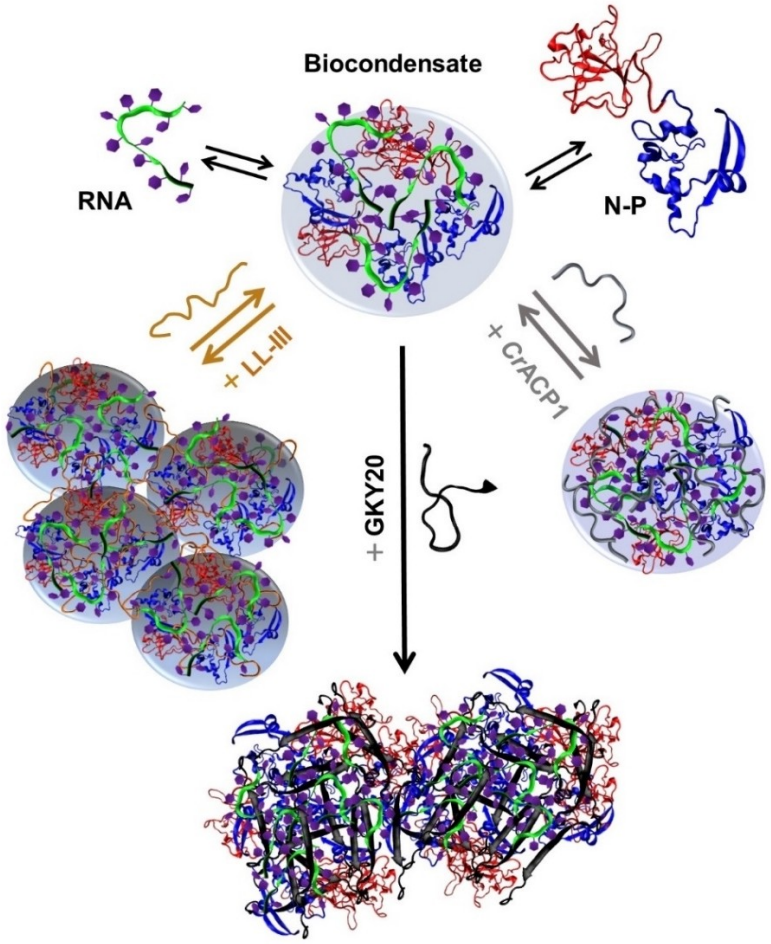

Figure 3. Schematic representation of the ability of AMPs to perturb N–P/polyU droplets. The peptide LL–III partitioning within the droplets promotes their reversible association, resulting in highly viscous condensate clusters. GKY20, on the other hand, induces irreversible formation of solid-like aggregates containing fibrillar structures. *Cr*ACP1 partitions into the condensates without affecting their morphology, but significantly slows down their dynamics.

with polyU within the droplets, as did LL–III and GKY20 (Figure 1D). Additional co-localization experiments of the FAM-labelled peptides with Alexa647-labelled N–P revealed that they are located in the same entities (Figure S4).

We then explored the effect of the three peptides on the dynamics of the N–P/polyU droplets by following the fluorescence recovery after photobleaching (FRAP) of Alexa647-labelled N–P. In the absence of the peptides (Figure 1C), a slow recovery of the fluorescence (from approx. 51 ± 2 % to approx. 84 ± 4 % after 200 s) was observed after bleaching the Alexa-N–P within the droplets, indicating relatively slow diffusion of the protein in and out the condensate. Interestingly, a similar observation was reported earlier[4] and attributed to the formation of immobilized N–P/RNA complexes which represent the first step of nucleocapsid assembly. Surprisingly, no significant fluorescence recovery was observed in the presence of LL–III and GKY20 (Figure 1D), revealing that N–P diffusion was strongly hindered. Conversely, the signal partially recovered (from approx. 27 ± 5 % to approx. 54 ± 6 % after 200 s, Figure 1D) in the presence of *Cr*ACP1, albeit to a much lower extent than for the neat N–P/polyU droplet phase. These results indicate that although the peptide *Cr*ACP1 does not cause morphological changes of the condensate, its incorporation into the condensate leads to a marked increase in the viscosity and thus to a significant reduction in the mobility of the N–P, which affects the dynamics within the droplets. The representative time-dependent behavior of photo-bleached N–P/polyU droplets in the absence and in the presence of the peptides is shown in Figure S5.

To gain more insight into the nature of the binding mechanism in the different droplet structures, we took microscopy images of the condensates (with and without peptides) after addition of 1,6-hexanediol and KCl, which serve as agents capable of modulating hydrophobic and electrostatic interactions (by charge screening), respectively (Figures S6, S7). In the absence of peptides, the addition of 1,6-hexanediol and KCl lead to partial dissolution of the N–P/polyU droplets due to a weakening of intermolecular interactions, as previously reported.[25] The SARS CoV-2 N–P is a highly basic protein, the surface of both NTD and CTD displaying highly positively charged regions, next to some negatively charged and neutral patches, which facilitate binding to nucleic acids. A similar result was observed for the LL–III-induced structures, indicating that clustering of N–P/polyU droplets in the presence of LL–III is

reversible. Conversely, neither 1,6-hexanediol nor salt could dissolve the aggregate structures induced by GKY20, revealing that it induces irreversible formation of solid-like aggregates. Conversely, both agents could dissolve the droplets containing *Cr*ACP1, indicating that the observed structures are still fluid-like droplets like those of neat N–P/polyU, albeit with greatly reduced dynamics induced by partitioning of the peptide.

At this stage, it was unclear whether the effects of the AMPs on N–P/polyU droplets are due to preferential interaction with one of the interacting partners or with both components. Consequently, we performed binding studies by recording anisotropy changes of FAM-labeled peptides upon addition of N–P or polyU in neat buffer and KCl-containing medium (Figures S8 and S9) in a concentration range where no phase separation occurs. The binding constants, K_b (in M^{-1}) determined for the pairwise interactions are summarized in Table 1. All the peptides bind to N–P in the absence of salt ($K_b \approx 10^5\ M^{-1}$). The addition of 0.5 M KCl lead to a 10-fold decrease of K_b for LL–III, while for GKY20 and *Cr*ACP1, the addition of KCl completely hampered the interaction. Further, both LL–III and GKY20 interact strongly with the RNA ($K_b \approx 10^7\ M^{-1}$), and a 1000-fold decrease in K_b was observed in the KCl-containing buffer. Instead, *Cr*ACP1 was shown to be unable to interact with polyU. It can therefore be concluded that LL–III and GKY20 establish interactions with both partners, N–P and polyU, while the slightly negatively charged *Cr*ACP1 only interacts with N–P.

To delve further into the nature of these interactions and establish whether the peptides can phase separate when mixed with N–P or polyU only, we performed corresponding light microscopy experiments (Figure S10). We found that N–P can also form droplets without RNA, albeit with a weaker tendency, as previously reported.[25] However, with polyU, the number of droplets was higher (Figure 1C), revealing that the RNA promotes phase separation.[4,5,25] The addition of LL–III and *Cr*ACP1 did not affect the droplet phase of N–P significantly, while GKY20 promoted droplet formation, suggesting direct interaction with N–P. When LL–III was mixed with polyU, liquid droplet formation took place as well, but no clustering of droplets as observed when N–P was also present, signifying that droplet condensation requires the interaction of the peptide with both N–P and polyU. Conversely, GKY20 and polyU formed the same aggregates as observed for the N–P/polyU system (Figure 1D), suggesting that the peptide-RNA interaction is the main driving force. Although LL–III and GKY20 show comparable net positive charges and affinities towards polyU, their impact on droplet formation is different, GKY20 being able to induce marked droplet aggregation with RNA alone. A comparison of their sequences (Figure 1B) shows that LL–III has similar residue types of the C-terminal region of GKY20, suggesting that the different behavior of the peptides is due to the N-terminal region of GKY20 which provides more hydrophobic residues. As a test, we recorded microscopy images of polyU with a peptide consisting of the last 10 residues of GKY20 (named C-GKY20) only (Figure S11). Only condensate formation was observed, and no aggregates were formed, suggesting that the N-terminal region with its hydrophobic residues is important for the aggregation propensity. *Cr*ACP1 had no discernible effect on polyU and did not form droplets, as expected due to the negligible interaction strength between the two molecules.

To further investigate the differences among the peptides in their interaction with N–P and polyU, we used circular dichroism (CD) spectroscopy, which allowed us to assess their conformation in the complexes. Figure 2 depicts the CD spectra of the three peptides recorded in the presence of N–P and polyU. The CD spectra of the peptides, N–P, and polyU alone are also reported. In accordance with the literature, the CD spectrum of N–P shows the features of an essentially α-helical structure with the presence of some other secondary structure elements (β-sheets and unordered structures).[26] Instead, all the AMPs adopt a random coil-like structure. For the N–P/peptide and polyU/peptide complexes with LL–III and *Cr*ACP1, we did not observe any significant conformational changes. The CD spectra of the peptides mixed with N–P (or polyU) showed the same features as those obtained from the sum of the spectra of peptides and N–P (or polyU) recorded separately. The interaction of GKY20 with N–P also occurred without visible conformational changes. Only for GKY20-polyU did we observe a CD spectrum that is indicative of the presence of β-sheet structures, suggesting that the observed aggregates are formed by fibril-like structures. To confirm this, we performed an atomic force microscopy (AFM) experiment of GKY20 mixed with polyU (inset of Figure 2B, right, and Figure S12). The AFM image clearly shows the presence of fibrillar structures with diameters of about 10–20 nm, most of which being strongly entangled in large aggregates.

In summary, we found that AMPs are able to markedly interfere with condensates formed by the SARS-CoV-2 N-protein and RNA (Figure 3), depending on the characteristics of the peptides, i.e., their sequence and amino acid types, which control their partitioning into the droplets and the morphological transformation of the condensates. The AMP LL–III

Table 1. Binding constants, K_b, for the interaction between the antimicrobial peptides and N–P or polyU in neat buffer and in the presence of KCl.

	N-Protein		PolyU	
Peptide	K_b / M^{-1} Buffer	K_b / M^{-1} 0.5 M KCl	K_b / M^{-1} Buffer	K_b / M^{-1} 0.5 M KCl
LL–III	$(2.9 \pm 0.4) \cdot 10^5$	$(5.2 \pm 1.8) \cdot 10^4$	$(6.4 \pm 0.9) \cdot 10^7$	$(9.9 \pm 5.3) \cdot 10^4$
GKY20	$(4.0 \pm 0.6) \cdot 10^5$	N.D.	$(8.1 \pm 1.1) \cdot 10^7$	$(4.1 \pm 2.1) \cdot 10^4$
*Cr*ACP1	$(9.1 \pm 2.3) \cdot 10^4$	N.D.	N.D.	N.D.

N.D. = not determinable.

partitions into the N–P/polyU droplets, promotes their association and reduces the dynamics of the N–P markedly. Instead, GKY20, through its additional hydrophobic N-terminal region, induces irreversible formation of solid-like fibrillar structures. *Cr*ACP1 partitions into the droplets without affecting their morphology, modulating their viscosity and dynamics, only. Further studies are desirable to decipher the role played by a given sequence (e.g., using scrambled sequences) and to understand the molecular determinants responsible for their partitioning within the condensates and the observed morphological transformations. The disturbance of such biomolecular condensates, which can, for example, lead to amyloid species (e.g., of FUS, PrP, α-synuclein, p53),[27–30] is a common hallmark of many diseases and hence represents a potential target for new treatments.[29,30] It has been pointed out that such condensates may be selectively disrupted by small-molecule drugs, suggesting a novel therapeutic route for cancers where dysregulated condensates contribute to the oncogenic state.[29] In recent decades, the discovery of AMPs as an excellent candidate to overcome antibiotic resistance has received significant attention. Here we have shown that AMPs can also modulate the droplet formation of the viral N–P protein. Alteration of droplet morphology and dynamics is expected to interfere with the normal functionality of the N–P biocondensate, thereby blocking or slowing down RNA transcription and consequently virion assembly. These results could pave the way for the development of a new class of AMP-based antiviral compounds targeting biocondensates.

Acknowledgements

R.W. acknowledges funding from the Deutsche Forschungsgemeinschaft (DFG, German Research Foundation) under Germany's Excellence Strategy – EXC 2033 – project number 390677874-RESOLV. R.O. is grateful to the Italian MUR for being granted a research associated position (PON R&I 2014–2020, CUP: E65F21003250003). Open Access funding enabled and organized by Projekt DEAL.

Conflict of Interests

The authors declare no conflict of interest.

Data Availability Statement

The data that support the findings of this study are available from the corresponding author upon reasonable request.

Keywords: SARS-CoV-2 nucleocapsid protein · liquid-liquid phase separation · antimicrobial peptides

[1] M. Mohamadian, H. Chiti, A. Shoghli, S. Biglari, N. Parsamanesh, A. Esmaeilzadeh, *J. Gene Med.* **2021**, *23*, e3303.
[2] P. Zhou, X.-L. Yang, X.-G. Wang, B. Hu, L. Zhang, W. Zhang, H.-R. Si, Y. Zhu, B. Li, C.-L. Huang, H.-D. Chen, J. Chen, Y. Luo, H. Guo, R.-D. Jiang, M.-Q. Liu, Y. Chen, X.-R. Shen, X. Wang, X.-S. Zheng, K. Zhao, Q.-J. Chen, F. Deng, L.-L. Liu, B. Yan, F.-X. Zhan, Y.-Y. Wang, G.-F. Xiao, Z.-L. Shi, *Nature* **2020**, *579*, 270–273.
[3] R. McBride, M. Van Zyl, B. Fielding, *Viruses* **2014**, *6*, 2991–3018.
[4] A. Savastano, A. Ibáñez De Opakua, M. Rankovic, M. Zweckstetter, *Nat. Commun.* **2020**, *11*, 6041.
[5] H. Chen, Y. Cui, X. Han, W. Hu, M. Sun, Y. Zhang, P.-H. Wang, G. Song, W. Chen, J. Lou, *Cell Res.* **2020**, *30*, 1143–1145.
[6] Z. Bai, Y. Cao, W. Liu, J. Li, *Viruses* **2021**, *13*, 1115.
[7] M. Fatima, M. A. S. Abourehab, G. Aggarwal, G. K. Jain, A. Sahebkar, P. Kesharwani, *Drug Discovery Today* **2022**, *27*, 103353.
[8] V. Teixeira, M. J. Feio, M. Bastos, *Progr. Lipid Res.* **2012**, *51*, 149–177.
[9] G. Guidotti, L. Brambilla, D. Rossi, *Trends Pharmacol. Sci.* **2017**, *38*, 406–424.
[10] M. Hassan, T. W. Flanagan, N. Kharouf, C. Bertsch, D. Mancino, Y. Haikel, *Pharmaceutica* **2022**, *15*, 72.
[11] R. Z. Essa, Y. Wu, K. Batumalaie, M. Sekar, C. Poh, *Pharmacol. Rep.* **2022**, *74*, 1166–1181.
[12] G. Jaiswal, V. Kumar, *PLoS One* **2020**, *15*, e0240004.
[13] W. T. Harvey, A. M. Carabelli, B. Jackson, R. K. Gupta, E. C. Thomson, E. M. Harrison, C. Ludden, R. Reeve, A. Rambaut, COVID-19 Genomics UK (COG-UK) Consortium, S. J. Peacock, D. L. Robertson, *Nat. Rev. Microbiol.* **2021**, *19*, 409–424.
[14] D. C. Dinesh, D. Chalupska, J. Silhan, E. Koutna, R. Nencka, V. Veverka, E. Boura, *PLoS Pathog.* **2020**, *16*, e1009100.
[15] Y. Peng, N. Du, Y. Lei, S. Dorje, J. Qi, T. Luo, G. F. Gao, H. Song, *EMBO J.* **2020**, *39*, e105938.
[16] V. Čeřovský, M. Buděšínský, O. Hovorka, J. Cvačka, Z. Voburka, J. Slaninová, L. Borovičková, V. Fučík, L. Bednárová, I. Votruba, J. Straka, *ChemBioChem* **2009**, *10*, 2089–2099.
[17] J. Slaninová, V. Mlsová, H. Kroupová, L. Alán, T. Tůmová, L. Monincová, L. Borovičková, V. Fučík, V. Čeřovský, *Peptides* **2012**, *33*, 18–26.
[18] R. Oliva, S. K. Mukherjee, Z. Fetahaj, S. Möbitz, R. Winter, *Chem. Commun.* **2020**, *56*, 11577–11580.
[19] R. Oliva, S. K. Mukherjee, L. Ostermeier, L. A. Pazurek, S. Kriegler, V. Bader, D. Prumbaum, S. Raunser, K. F. Winklhofer, J. Tatzelt, R. Winter, *Chem. Eur. J.* **2021**, *27*, 11845–11851.
[20] S. M. Mandal, L. Migliolo, S. Das, M. Mandal, O. L. Franco, T. K. Hazra, *J. of Cellular Biochemistry* **2012**, *113*, 184–193.
[21] S. E. Farr, E. J. Woods, J. A. Joseph, A. Garaizar, R. Collepardo-Guevara, *Nat. Commun.* **2021**, *12*, 2883.
[22] G. Kasetty, P. Papareddy, M. Kalle, V. Rydengård, M. Mörgelin, B. Albiger, M. Malmsten, A. Schmidtchen, *Antimicrob. Agents Chemother.* **2011**, *55*, 2880–2890.
[23] R. Oliva, P. Del Vecchio, A. Grimaldi, E. Notomista, V. Cafaro, K. Pane, V. Schuabb, R. Winter, L. Petraccone, *Phys. Chem. Chem. Phys.* **2019**, *21*, 3989–3998.
[24] D. Wlodkowic, J. Skommer, Z. Darzynkiewicz, in *Mammalian Cell Viability* (Ed.: M. J. Stoddart), Humana Press, Totowa, NJ, **2011**, pp. 81–89.
[25] S. M. Cascarina, E. D. Ross, *J. Biol. Chem.* **2022**, *298*, 101677.
[26] S. M. Kelly, T. J. Jess, N. C. Price, *Biochim. Biophys. Acta BBA-Proteins Proteomics* **2005**, *1751*, 119–139.
[27] S. Cinar, H. Cinar, H. S. Chan, R. Winter, *J. Am. Chem. Soc.* **2019**, *141*, 7347–7354.
[28] H. Cinar, Z. Fetahaj, S. Cinar, R. M. Vernon, H. S. Chan, R. H. A. Winter, *Chem. Eur. J.* **2019**, *25*, 13049–13069.
[29] J. L. Silva, D. Foguel, V. F. Ferreira, T. C. R. G. Vieira, M. A. Marques, G. D. S. Ferretti, T. F. Outeiro, Y. Cordeiro, G. A. P. De Oliveira, *Chem. Rev.* **2023**, *123*, 9094–9138.
[30] A. Boija, I. A. Klein, R. A. Young, *Cancer Cell* **2021**, *39*, 174–192.

Manuscript received: January 5, 2024
Accepted manuscript online: March 14, 2024
Version of record online: April 10, 2024